Far-Infrared Spectroscopy of Quantum Wires and Dots, Breaking Kohn's Theorem

D. Heitmann, K. Bollweg, V. Gudmundsson*, T. Kurth, and S. P. Riege
Institut für Angewandte Physik und Zentrum für Mikrostrukturforschung, Universität Hamburg, Jungiusstraße 11, D-20355 Hamburg, Germany.
**Science Institute, University of Iceland, Dunhaga 3, IS-107 Reykjavik, Iceland.*

We review far-infrared experiments on quantum wires and dots. In particular we shows that with tailored deviations from a parabolic external lateral confinement potential one can break Kohn's theorem. This allows a detailed investigation of the internal relative motion in quantum dots and wires and the study of electron-electron interaction effects, for example the formation of compressible and incompressible states in quantum dots and antidots.

Quantum dots and wires [1,2] can advantageously be prepared starting from layered semiconductor systems, for example, from MBE grown AlGaAs-GaAs heterostructures or quantum wells. In these systems one can tailor with the preparation and by external electric and magnetic fields the electron density and the potential and thus study in detail electron-electron (ee) interaction and confinement effects. Far infrared (FIR) spectroscopy is a direct way to investigate the dynamic excitations in these low dimensional systems. [1–11] It turns out that the dynamic response exhibits an interesting complex interplay of atomic-like single-particle and many-body effects. This arises in particular from the fact that, due to electrostatic reasons, the external confining potential in such structures has a nearly parabolic shape, as we will explain in detail below.

The unique and important point of a parabolic external confinement is, as has been shown for quantum wells [12], and quantum dots [13], that the Hamiltonian for an N-electron system including ee-interaction

$$H_N = \sum_{j=1}^{N} H(\vec{r_j}, \vec{p_j}) + \sum_{i<j} v(\vec{r_i} - \vec{r_j}) \tag{1}$$

separates into a center-of-mass (CM) motion, $(\vec{R}, \vec{P})$, and relative internal motion, $(\vec{r}_{j,\mathrm{rel}}, \vec{p}_{j,\mathrm{rel}})$.

$$H_N = H(\vec{R}, \vec{P}) + H_{\mathrm{rel}}(\vec{r}_{j,\mathrm{rel}}, \vec{p}_{j,\mathrm{rel}}) \tag{2}$$

where

$$H(\vec{r}, \vec{p}) = \frac{1}{2m^*}\left[\vec{p} + \frac{e}{c}\vec{A}(\vec{r})\right]^2 + \frac{1}{2}m^*\Omega_0^2 r^2 \tag{3}$$

is a single-particle Hamiltonian, here for dots with the potential $V(\vec{r}) = \frac{1}{2}m^*\Omega_0^2\vec{r}^2$. The decoupled CM motion exactly describes the one-electron Hamiltonian of the external potential. The wavelength of the FIR radiation (typically 100 μ) is much larger than the size of the quantum structures, 100 nm. Thus FIR excitations can be described very well by dipole excitation. Since the dipole excitation only couples to the CM motion, which is totally decoupled from the relative motion, the optical dipole response of a quantum structure with parabolic confinement represents a rigid collective CM excitation with transition frequencies corresponding to the single-particle energies of the bare external potential. This statement is called the 'Generalized Kohn's Theorem', generalizing Kohn's results for electrons in a translationally invariant system. [14]

The one-particle energies in a quantum wire with a parabolic external potential $V(x) = \frac{1}{2}m^*\omega_0^2 x^2$ are

$$E_n = \sqrt{(\hbar\omega_0)^2 + (\hbar\omega_c)^2}\ \left(n + \frac{1}{2}\right) \tag{4}$$

thus the dipole allowed transitions have frequencies:

$$\omega_r^2(B) = \omega_0^2 + \omega_c^2. \tag{5}$$

For dots we have in a magnetic field B for a parabolic potential the one-particle energy spectrum [15]

$$E_{n,\ell} = (2n + |\ell| + 1) \cdot \sqrt{(\hbar\Omega_0)^2 + (\hbar\omega_c/2)^2}\ +\ \ell \cdot \hbar\omega_c/2 \tag{6}$$

where n= 0,1,2 ... and $\ell = 0, \pm 1, \pm 2 ...$ are, respectively, the radial and the azimuthal quantum numbers. From calculations of the matrix elements one finds that dipole allowed transitions have transition energies

$$\omega_\pm = \sqrt{\Omega_0^2 + (\omega_c/2)^2} \pm \omega_c/2. \tag{7}$$

In the following we will first review experiments [10], which allow us to characterize the external potential of experimental etched quantum wires. We will discuss experiments which show that, for parabolic potentials, indeed Kohn's theorem holds. However, we will also demonstrate that it is possible to prepare tailored deviations from a parabolic confinement, which give us access to the internal relative motion of electrons in quantum structures and thus allow us to study ee interaction effects. We will in particular discuss the formation of compressible and incompressible states in quantum dots and antidots. [11] Such states are currently extensively

investigated, both theoretically [16–19] and experimentally [20], in particular to explain transport phenomena in the quantum Hall regime.

A direct way to realize quantum structures is to prepare a suitable mask on top of a heterostructure or quantum well and to etch all the way through the active layer. This process is called 'deep-mesa etching'. For modulation-doped systems GaAs has the very advantageous property that at a clean surface the Fermi level is pinned near the mid gap. Microscopically, this means that surface states trap electrons. These negative surface charges in the etched sidewalls repel the free carriers in the wire, in other words, the active electron channel is separated by a lateral depletion length, which is typically 50 to 200 nm (see e.g. Ref. [4]). This sidewall depletion is a great advantage, because higher Fourier components of the confining electric field, which may arise from fabrication-induced sidewall fluctuations, are effectively suppressed.

We prepared arrays of quantum wires with geometrical width $w = 160$ nm to 350 nm starting from MBE-grown modulation-doped GaAs/AlGaAs samples. A photoresist etching mask consisting of an array of parallel submicron wires was prepared by holographic lithography techniques, and this mask was transfered into the heterostructure by an $SiCl_4$ reactive ion etching process. The etch depth was $h = 110$ nm. An electron micrograph of a quantum wire array is shown in Fig. 1a. For the following discussion we define an effective donor density $\rho_+^{\rm eff}$, effective in the sense that only donors providing electrons in the quantum well are considered. Those donors which contribute electrons to the surface of the GaAs cap layer are electrostatically compensated by the latter ones. If d_+ is the thickness of the donor layer, we have $n_{2D} = d_+\rho_+^{\rm eff}$. For the etched quantum wires we find that below a critical wire width $w_{\rm crit} = 200$ nm no FIR response could be detected. This means that all net charges provided by the donors in the original 2D quantum well to the GaAs are now transfered into the surface states in the sidewalls. From this we can determine the number of surface charges per wire length on each sidewall as $\lambda_- = \frac{1}{2} w_{\rm crit} n_{2D} = 4.1 \cdot 10^6$ cm^{-1}, or, if we assume that these surface states are distributed homogeneously over the sidewall with etch depth h we get a surface density $\sigma_- = \lambda_-/h = 3.7 \cdot 10^{11}$ cm^{-2}. If we increase the wire width $w > w_{\rm crit}$ we get mobile electrons in the 1D channel with a 1D density $n_{1D} = (w - w_{\rm crit}) d_+ \rho_+^{\rm eff}$. The determination of the surface charge density σ_- from $w_{\rm crit}$ and the knowledge of the donor density $\rho_+^{\rm eff}$ as determined from the 2D samples allow us to perform an electrostatic calculation of the external potential using the external charges as sketched in Fig. 1b.

The calculated potentials for different w, using σ_-, $\rho_+^{\rm eff}$, and h as defined above, are plotted in Fig. 2a. It shows that the potential is indeed nearly parabolic. To characterize this potential and to compare it with the FIR experiment we approximate it by the expression

$$V(x) = \frac{1}{2}\hbar\omega_0 \left[\left(\frac{x}{l_0}\right)^2 + a\left(\frac{x}{l_0}\right)^4 + b\left(\frac{x}{l_0}\right)^6 \right] \qquad (8)$$

with $l_0 = \sqrt{\hbar/(m^*\omega_0)}$. The parameters ω_0, a, and b in their dependence on w, as determined from fits of (8) to the calculated potential, are shown by the solid lines in Fig. 2b-c.

We have also performed FIR transmission spectroscopy on these quantum wires. The temperature was 4.2 K and a perpendicular magnetic field B was applied. Experimental details are described e.g. in Refs. [4,11]. FIR spectra for the quantum wire array are shown in Fig. 3a. The B dispersion of the resonance positions is plotted for three arrays with different geometrical widths w in Fig. 3b-c. The dispersion shown in Fig. 3b is exactly the dispersion expected from eq. (5). This implies that in this sample the potential is indeed nearly parabolic and we can determine the external potential from the resonance position at $B = 0$. In Fig. 2b we compare this frequency $\omega_r(B = 0)$, as determined in this totally independent FIR experiment, with the result from the electrostatic calculations. There is a very good agreement both for the absolute values as well as for the trend of the w-dependence. Note that we do not use any adjustable parameters in our evaluation. This shows that our electrostatic model is a good model and well suited for a simple characterization of the potential in etched quantum wires.

An interesting observation is that in Fig. 3c an anticrossing occurs. The observation of such an anticrossing shows that the potential for the wider quantum wells is not strictly parabolic. The origin of the anticrossing is the so-called non-local interaction with Bernstein modes which has been observed also in other experiments, e.g., [7,9], and has been discussed extensively e.g. by Gudmundsson et.al. [21]. Another type of anticrossing and higher order modes have been observed for square shaped quantum dots, indicating again nonparabolic external confinement [6]. We will not elaborate on these experiments here, but we like to discuss another very interesting ee-interaction phenomenon, the formation of compressible and incompressible states in quantum dots and wires and its investigation with FIR spectroscopy.

The formation of compressible and incompressible states is one of the currently most intensively discussed phenomena in the field of mesoscopic systems and semiconductor microstructures. It was proposed by Beenakker [16] and Chklovskii et.al. [17] that the electron density near the edge of a two-dimensional electron system (2DES) in the presence of a magnetic field B exhibits, to a certain degree, a steplike density profile $N_s(r)$ arising from the self-consistent and B-dependent formation of incompressible stripes, where the 2D density $N_s(r)$ is fixed at integer filling factors ν, i.e. $N_s(r) = \nu \cdot \frac{eB}{h}$, and compressible stripes, where $N_s(r)$ can vary. r is the direction perpendicular to the edge in the 2D

plane. This many-body effect has an important influence on the transport properties in the integer and fractional quantum Hall effect. [20] It also leads to new phenomena as e.g. composite droplets and edge reconstructions in few-electron systems. [18,19].

We have prepared antidot and dot arrays starting from modulation-doped AlGaAs – GaAs double-layered quantum-well structures. [11] The width of both quantum wells was 7.0 nm, separated by a 55 nm barrier. Three doping layers, one on the top of the upper quantum well, one in the barrier and one below the lower quantum well were separated by 15 nm spacers on each side. The electron density of the 2DES was about $N_s = 9 \cdot 10^{11}$ cm^{-2} in each well. We concentrate here on one antidot sample with a period of $a = 800$ nm in both lateral directions and a geometrical hole radius of $R_g = 180$ nm (determined from electron micrographs) and on a dot array with the same period and the same geometrical radius and about 750 electrons per well in each dot. The double-layer dots and antidots with high electron densities in our experiments increase the signal strength and, moreover, the three doping layers increase the external potential and thus the frequencies, in particular also of the low frequency mode. They also produce a non parabolic hard wall type confining potential which makes our experiments sensitive to ee-interaction.

The experimental dispersions for the antidot and dot array are depicted in Fig. 4. Both samples show two strong modes. For the dot array both modes start for $B = 0$ at $\omega = 86$ cm^{-1}. With increasing B the upper mode ω_+ approaches the cyclotron resonance $\omega_c = \frac{eB}{m^*}$ (m^* is the effective mass) of the 2DES. The lower branch, ω_-, decreases in frequency. This is, on a first sight, exactly the behavior expected from eq. (7). For the antidot sample the modes are separated by a gap. The ω_- mode starts close to ω_c, it increases at small B and then, above $B \approx 8\ T$, decreases in frequency. This two-mode-behavior has been observed before. [5–8] The low frequency ω_- mode represents at larger B a collective edge magnetoplasmon type of excitation where the individual electrons perform skipping orbits inside the *inner* circumference of the dot. For the antidot array the ω_- mode at large B represents a similar type of collective motion, in this case the skipping orbit occurs at the *outer* circumference of the antidot. With decreasing B and thus large cyclotron radius r_c the electrons can eventually perform classical cyclotron motion around the antidots. Then ω_- decreases and approaches ω_c.

What is surprising and was observed for the first time in Ref. [11] for dot and antidot arrays, is the oscillatory behavior of the resonance frequency. If we plot the frequencies of the low frequency antidot mode versus the inverse magnetic field B^{-1} we find that both the maxima and minima of the resonance frequency are periodic in B^{-1}. We can relate them to the filling factor $\nu = \frac{N_s h}{eB}$ with $N_s = 9 \cdot 10^{11}$ cm^{-2} which agrees within the experimental accuracy with the Shubnikov-de Haas (SdH) measurements of N_s. We find that maxima occur at half filled Landau levels (ν odd) and minima for fully occupied Landau levels (ν even). Spin splitting is not resolved for our experimental conditions. The interesting finding is that for the dots the maxima and minima of the eigenfrequencies are again filling factor related, however, with an opposite behavior as compared to the antidot array. For dots we observe at fully occupied Landau levels maxima and at half filled Landau levels minima in the frequency.

To explain this behavior we have performed self-consistent Hartree calculations of the eigenstates and the density profile for a single-layer dot containing N = 60 electrons. We assume a degeneracy of $\frac{eB}{h}$ per Landau level and model the nonparabolic potential, similarly as in eq. (8), by $V(r) = \frac{1}{2}\hbar\omega_0\{(r/l_0)^2 + a(r/l_0)^4\}$ with $\hbar\omega_0 = 3.37$ meV, $m^* = 0.067 m_e$, $a = 0.0674$, and $l_0 = \sqrt{\hbar/(m^*\omega_0)}$; T is 1.0 K. The calculation techniques are described in [21]. In Fig. 4a we show the resulting density profile $N_s(r)$. At $B = 4.9$ T we have a pronounced formation of regions with flat densities indicating the incompressible regimes. For $B = 3.7$ T, when the filling factor in the middle of the dot has not an even value, the density profile smoothes out, indicating a suppression of the incompressible states. An even more pronounced oscillatory density profile has been calculated for quantum wire in the quantum Hall regime by Chakraborty et.al [19]. Starting from the Hartree energies we have calculated within RPA the ω_- FIR resonance frequency. In Fig. 5b we see that the filling factor depending formation of the compressible and incompressible stripes leads indeed to frequency oscillations with exactly the same phase as in the experiment, e.g. a maximum in the resonance frequency at full filling in the 'bulk', if we call the center of the dot the 'bulk' region. This confirms our experiments and interpretation. An oscillatory behavior has also been calculated by Darnhofer et. al. [22]

So far there is no equivalent self-consistent calculation for antidot arrays. We have explained in detail in Ref. [11] that one expects in antidots, which are a reversed structure with respect to the dots, exactly the reverse phase for the oscillation. This is indeed observed in the experiments. It also shows that the oscillations do not arise from some extrinsic Shubnikov-de Haas type of effect, but are an intrinsic property of the ee-interaction in quantum dots and antidots.

Besides using a nonparabolic potential we can break Kohn's theorem, and thus study the internal ee-interaction, also by various others means. Darnhofer and Rössler [23] have shown that a nonparabolic bandstructure, meaning, a nonquadratic k-dependence in the energy dispersion in eq. (1), produces a quite similar type of anticrossing behaviors as discussed above. One can also perform Raman experiments, where it is easy to investigate excitations with wavevector transfers $q > 0$. This is a non-dipole excitation. We refer here to a recent paper and the references within this paper on Raman experiments on quantum wires, where various types

of internal ee-interaction phenomena have been investigated. [24] Another way to break Kohn's theorem are experiments in tilted magnetic fields. [25] Here the coupling with the - nonparabolic - original 2D confinement in growth direction leads to coupling with internal motion. Very interesting effects like shellstructures have recently been observed in quantum dots prepared by the novel self-assembling techniques. [26]

We acknowledge the cooperation with many colleagues, as listed in the original references, and support by the German Science Foundation through the Graduiertenkolleg 'Nanostrukturierte Festkörper' and Sonderforschungsbereich 508 'Quantenmaterialien', and the Icelandic Science Foundation.

Within the allotted space we can give here only a very brief list of reference. For more references we refer to the original paper and extended reviews, e.g. [1,2]

[1] D. Heitmann and J.P. Kotthaus, Physics Today **46**, 56 (June 1993).

[2] D. Heitmann in *Confined electrons and phonons*, Plenum Press, Series B: Physics Vol. 340, New York and London, 1995, eds. E. Burstein and C. Weisbuch, p. 305.

[3] W. Hansen, M. Horst, J. P. Kotthaus, U. Merkt, Ch. Sikorski, and K. Ploog, Phys. Rev. Lett. **58**, 2586 (1987).

[4] T. Demel, D. Heitmann, P. Grambow, and K. Ploog, Phys. Rev. B **38**, 12732 (1988) and Appl. Phys. Lett. **53**, 2176 (1988).

[5] Ch. Sikorski and U. Merkt, Phys. Rev. Lett. **62**, 2164 (1989).

[6] T. Demel, D. Heitmann, P. Grambow, and K. Ploog, Phys. Rev. Lett **64**, 788 (1990).

[7] K. Kern, D. Heitmann, P. Grambow, Y.H. Zhang, and K. Ploog, Phys. Rev. Lett. **66**, 1618 (1991).

[8] B. Meurer, D. Heitmann, and K. Ploog, Phys. Rev. Lett. **68**, 1371 (1992).

[9] H. Drexler, W. Hansen, J. P. Kotthaus, M. Holland, and S. P. Beaumont, Phys. Rev. B **46**, 12 849 (1992).

[10] S. P. Riege, T. Kurth, F. Runkel, D. Heitmann, and K. Eberl, Appl. Phys. Lett. **70**, 111 (1997).

[11] K. Bollweg, T.Kurth, D.Heitmann, V. Gudmundsson, E. Vasiliadou, P. Grambow, and K. Eberl, Phys. Rev. Lett **76**, 2774 (1996).

[12] L. Brey, N. Johnson, and B. Halperin, Phys. Rev. B **40**, 10647 (1989).

[13] P. Maksym and T. Chakraborty, Phys. Rev. Lett. **54**, 108 (1990).

[14] W. Kohn, Phys. Rev. **123**, 1242 (1961).

[15] V. Fock, Z. Phys., **47**, 446 (1928).

[16] C. W. Beenakker, Phys. Rev. Lett. **64**, 216 (1990).

[17] D. B. Chklovskii, B. I. Shklovskii, and L. I. Glazman, Phys. Rev. B **46**, 4026 (1992).

[18] X. G. Wen, Phys. Rev. Lett. **64**, 2206 (1990); M. D. Johnson and A.H. MacDonald, Phys. Rev. Lett. **67**, 2060 (1991); K. Lier and R. R. Gerhards, Phys. Rev. B **50**, 7757 (1994); J. H. Oaknin, L. Martin-Moreno, J. J. Palacios, and C. Tejedor, Phys. Rev. Lett. **74**, 5120 (1995).

[19] T. Chakraborty, K. Niemelä, and P. Pietiläinen, Phys. Rev. Lett.**78**, 4829 (1997).

[20] P. L. Mc Euen, E. B. Foxman, J. Kinaret, U. Meirav, M. A. Kastner, N. S. Wingreen, and S. J. Wind, Phys. Rev. B **45**, 11419 (1992), R. J. F. van Haren, F. A. P. Blom, and J. H. Wolter, Phys. Rev. Lett. **74**, 1198 (1995), N. B. Zhitenev, R. J. Haug, K. v. Klitzing, and K. Eberl, Phys. Rev. Lett. **71**, 2292 (1993).

[21] V. Gudmundsson, A. Brataas, P. Grambow, B. Meurer, T. Kurth, and D. Heitmann, Phys. Rev. B **51**, 17744 (1995).

[22] T. Darnhofer, M. Suhrke, and U. Rössler Europhys. Lett. **35**, 591 (1996).

[23] T. Darnhofer and U. Rössler, Phys. Rev. B **47**, 16020 (1993).

[24] C. Steinebach, R. Krane, G. Biese, C. Schüller, D. Heitmann, and K. Eberl, Phys. Rev. B **54**, R14281 (1996).

[25] B. Meurer, D. Heitmann, and K. Ploog, Phys. Rev. B **48**, 11488 (1993).

[26] M. Fricke, A. Lorke, J. P. Kotthaus, G. Medeiros-Ribeiro, and P. M. Petroff, Europhys. Lett. **36**, 197 (1996).

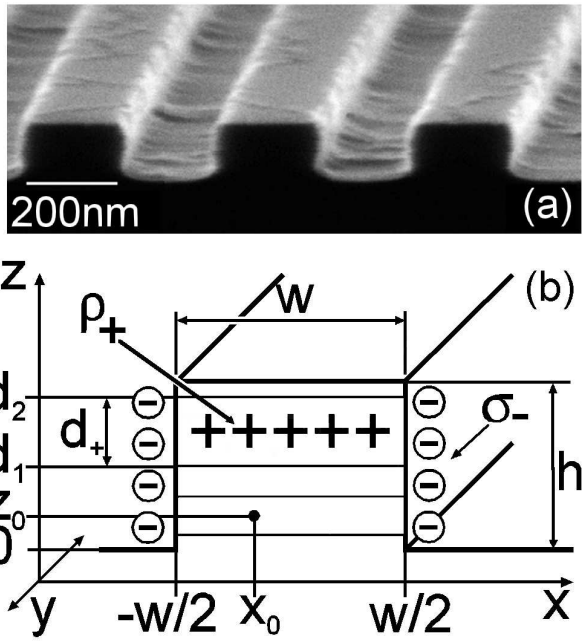

FIG. 1. (a) Micrograph of a quantum wire array. (b) Sketch of the quantum wire and the input parameters of our calculation. The donor layer extends from $z = d_1$ to $z = d_2$.

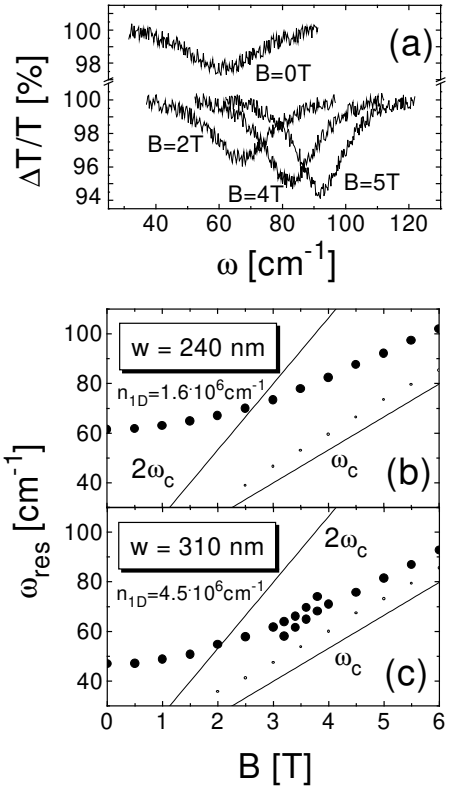

FIG. 2. (a) Electrostatic calculation of the external lateral potential for different wire widths (solid lines). The curves in (b)-(d) show fit parameters for a least-square fit with a sixth order polynomial, and the dashed lines in (a) give the parabolic part of the lateral potential. The measured resonance frequencies (solid dots) in (b) are in good agreement with the calculated value ω_0 of the electrostatic potential. This demonstrates Kohn's theorem.

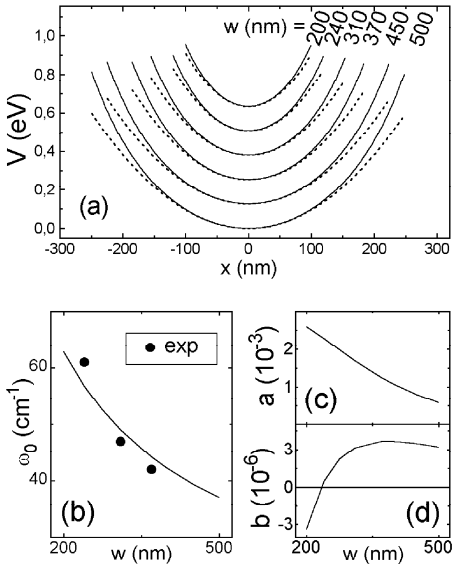

FIG. 3. (a) Experimental FIR spectra for quantum wire arrays. (b),(c) 1D intersubband FIR resonance position as a function of the magnetic field for quantum wires with different wire widths w.

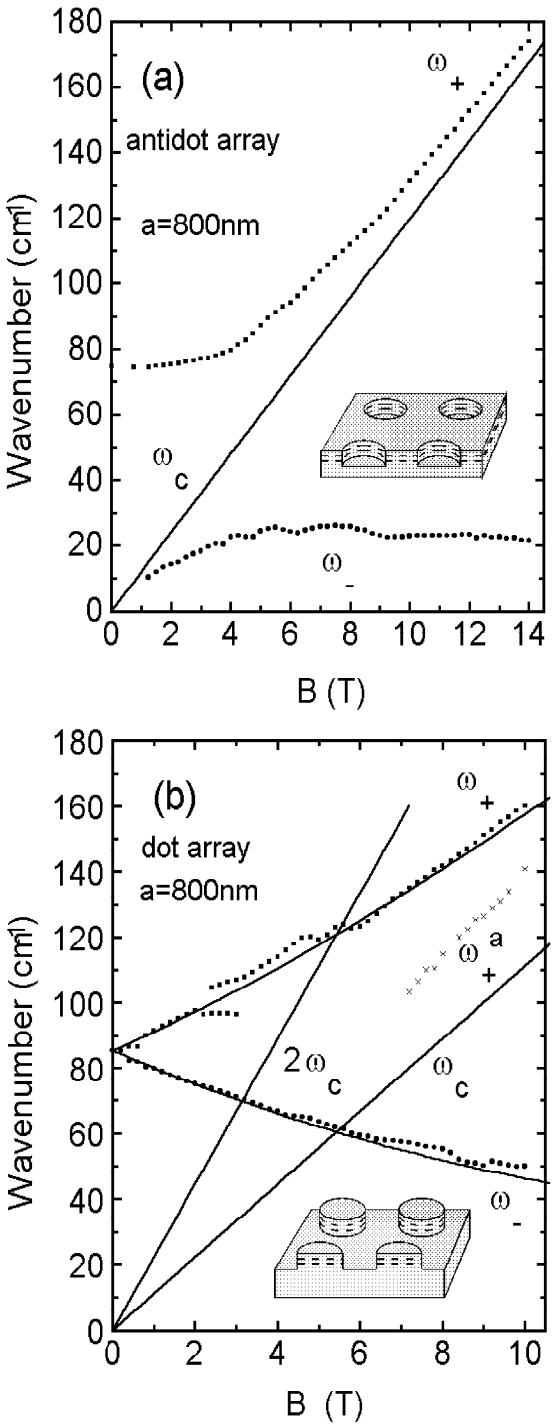

FIG. 4. Experimental dispersions of the resonance frequencies in an antidot (a) and dot array (b). The low frequency modes (ω_-) exhibit well pronounced oscillations. In (b) the straight curves represent a calculated dispersion $\omega_{\pm}^{ca}$ using eq. (7) with $\omega_0 = 86$ cm^{-1}. The mode labeled ω_+^a in (b) is the acoustic mode of the double-layered dot array. The anomalies at 126 cm^{-1} in (b) arises from $2\omega_c$ interaction [7,21] and at 100 cm^{-1} from ω_{+1}-ω_{-2}-interaction [6].

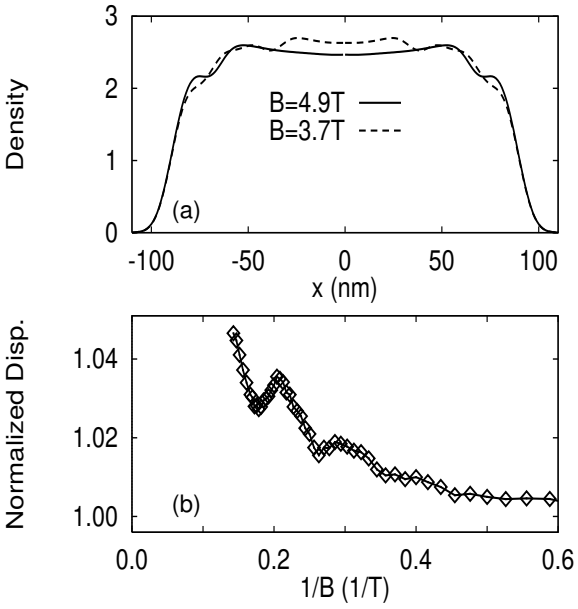

FIG. 5. (a) Hartree calculation of the density profile in a quantum dot in units of 10^{11} cm^{-2}. The flat regions for $B = 4.9$ T indicate the incompressible regimes. (b) Ratio of the RPA and the result eq.(7) for a parabolic potential ω_-/ω_-^{pa}, vs B^{-1}.